Enzyme-Catalyzed Condensation Reaction in a Mammalian α-Amylase. High-Resolution Structural Analysis of an Enzyme−Inhibitor Complex[†]

Minxie Qian,[‡,§] Virginie Nahoum,[‡] Jacques Bonicel,[∥] Hilmar Bischoff,[⊥] Bernard Henrissat,[‡] and Françoise Payan*[,‡]

Architecture et Fonction des Macromolécules Biologiques, UMR 6098, CNRS and Universities Aix-Marseille I and II, 31 Chemin Joseph Aiguier, 13402 Marseille, France, Bioénergétique et Ingénierie des Protéines, CNRS-IBSM, 31 Chemin Joseph Aiguier, 13402 Marseille, France, Institute of Physical Chemistry, Peking University, Beijing 100871, People's Republic of China, and Bayer AG, Institute for Cardiovascular and Arteriosclerosis Research, Wuppertal, Germany

Received January 31, 2001; Revised Manuscript Received April 27, 2001

ABSTRACT: Mammalian α-amylases catalyze the hydrolysis of α-linked glucose polymers according to a complex processive mechanism. We have determined the X-ray structures of porcine pancreatic α-amylase complexes with the smallest molecule of the trestatin family (acarviosine-glucose) which inhibits porcine pancreatic α-amylase and yet is not hydrolyzed by the enzyme. A structure analysis at 1.38 Å resolution of this complex allowed for a clear identification of a genuine single hexasaccharide species composed of two α-1,4-linked original molecules bound to the active site of the enzyme. The structural results supported by mass spectrometry experiments provide evidence for an enzymatically catalyzed condensation reaction in the crystal.

α-Amylase (α-1,4-glucan-4-glucanohydrolase, EC 3.2.1.1) catalyzes the hydrolysis of the α-(1,4)-glycosidic linkages of starch components, glycogen and various oligosaccharides. α-Amylase is a member of family 13 of the sequence-based classification of glycoside hydrolases (*1*). These families are now available at the web site http://afmb.cnrs-mrs.fr/~pedro/CAZY/db.html (*2*).

In an attempt to develop therapeutic strategies against diabetes, obesity, and hyperlipidemia, extensive research has been carried out with a view to identifying α-glucosidase inhibitors (*3*−*5*). Agents having inhibitory effects on pancreatic α-amylase and on the sucrase and maltase activities of intestinal disaccharidases were discovered in vitro in *Actinomycetes* broths (*6*) and found to give rise to a series of homologous pseudo-oligosaccharide compounds. These substances contain a specific structural entity named acarviosine (an unsaturated cyclitol unit linked to a 4,6-dideoxy-4-amino-D-glucose) (Figure 1), which is the essential structural unit responsible for the activity of all the inhibitors belonging to this family. This unit is linked by α-(1,4)-*O*-glycosidic bonds to a variable number of glucose residues. One particular compound, the pseudo-tetrasaccharide acarbose (in which the acarviosine unit is linked to a maltose molecule; Figure 1), is particularly well-known, since it is used against diabetic diseases. This molecule appears to be a potent inhibitor of α-amylases. Crystallographic methods have been extensively used to analyze the protein−carbohydrate inhibitor interactions. The strong inhibition is widely attributed to the binding of the cyclitol unit whose half-chair conformation mimics the substrate distortion expected in the transition state. The adjacent glycosidic bond is *N*-linked, preventing enzymatic hydrolysis. According to chemical and enzymatic studies of the degradation of the acarbose molecule, acid hydrolysis allows breakage of both *O*-glycosidic bonds, while enzymatic hydrolysis by α-amy-

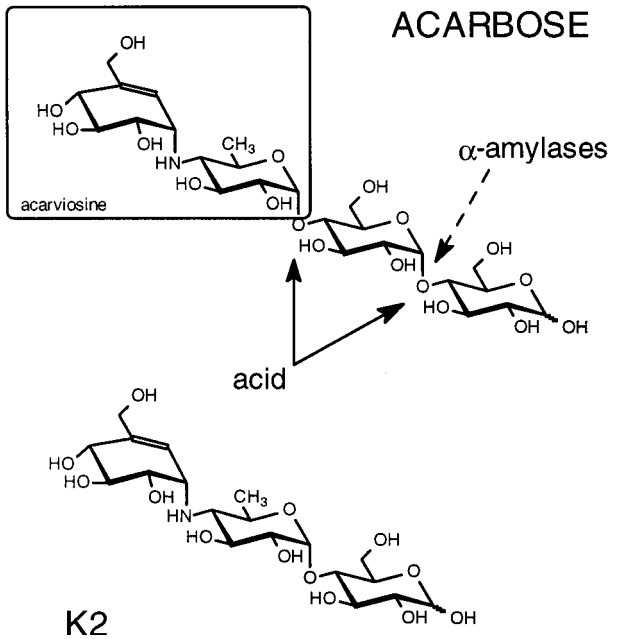

FIGURE 1: Chemical structures of acarbose and compound K2. The acarviosine moiety is boxed. The solid and dashed arrows indicate the sites of hydrolysis of acarbose by acid and α-amylases, respectively (*8*). Compound K2 is produced from acarbose by enzymatic removal of the glucose residue at the reducing end.

[†] This work was funded by CNRS and Bayer Pharma−Puteaux France.

* Corresponding author. Fax: 33 4 91 16 45 36; Email: payan@afmb.cnrs-mrs.fr.

[‡] Architecture et Fonction des Macromolécules Biologiques, CNRS and Universities Aix-Marseille I and II.

[§] Institute of Physical Chemistry, Peking University.

[∥] Bioénergétique et Ingénierie des Protéines, CNRS-IBSM.

[⊥] Bayer AG, Institute for Cardiovascular and Arteriosclerosis Research.

10.1021/bi0102050 CCC: $20.00
Published on Web 05/30/2001

lase only allows cleavage of the linkage between the two glucose units (Figure 1). Therefore, the glucose unit at the reducing end of the acarbose molecule can be easily cleaved away by α-amylases; the loss of this glucose unit yields a pseudo-trisaccharide, acarviosine-glucose, which is not degraded by pure preparations of α-amylases (*7, 8*). The K_i constant for acarbose to PPA[1] is 9.7×10^{-6} M (*9*). The inhibitory activity of the generated pseudo-trisaccharide compound has been reported to be only 1.7 times less than that of acarbose (*6*). This molecule, still highly active both in vivo and in vitro, constitutes the smallest component within the series of α-glucosidase inhibitors belonging to the trestatin family. It provides an important tool for investigation of the process, discussed at length and still not elucidated, which takes place in the active site of α-amylases and leads to the presence of an extended ligand species bound to the active site upon incubation of acarbose with the free enzyme. This molecule is referred to as compound K2 throughout this paper (Figure 1). We report here an analysis of the interaction between porcine pancreatic α-amylase and the K2 molecule used as a probe of the mechanism of this medically important enzyme.

Porcine pancreatic α-amylase (PPA) is an *endo*-type amylase. It catalyzes the hydrolysis of internal α-(1,4)-glucosidic bonds in amylose and amylopectin via a "multiple attack" process (processive degradation of the substrate) toward the nonreducing end (*10*). The enzyme requires one essential calcium ion (*11, 12*) to maintain its structural integrity, and it is activated by chloride ions (*13*). The three-dimensional molecular structure models of porcine (*14*) and human pancreatic (*15*) α-amylases are extremely similar and so are their interaction patterns with carbohydrate and proteinaceous inhibitors (*16*−*18*). The architecture of the pancreatic α-amylase (and shared by all other enzymes of the glycoside hydrolase family 13) consists of three domains: the catalytic core domain (A), comprising a $(\beta/\alpha)_8$ barrel, contains an extended loop inserted between the third β-strand and the third α-helix (called domain B, residues 100−169). The C-terminal domain (domain C, residues 405−496) forms a distinct globular unit with 10 β-strands forming a Greek key motif. Elements from domains A and B are involved in the architecture of the three most functionally important sites: the active site, the calcium binding site, and the chloride binding site. An atomic description of the interactions between the mammalian enzymes and carbohydrate inhibitors within the active site depression has been published along with the refined structures of PPA/acarbose complexes [which were determined using two different crystal forms (*16, 19*)] and HPA/acarbose complexes (*17, 18*). The X-ray structures clearly show that a subset of residues is directly involved in binding the inhibitor and/or is in a suitable position to assist the catalysis. The structural arrangement indicates that the requirements for hydrolysis to occur via the general acid hydrolysis mechanism are satisfied in the mammalian α-amylase structures. The widely recognized two-step mechanism originally proposed by Koshland (*20*) for retaining glycoside hydrolases requires the presence of two carboxyl-containing amino acids, one acting as an acid/base catalyst and the other as a nucleophile responsible for the formation of the glycosyl-enzyme intermediate (*21*). In view of our crystallographic data (*16*) (Figure 2), we suggested that both Asp197 and Glu233 may be required to produce the β-linked glycosyl-enzyme intermediate. McCarter and Withers confirmed the role of Asp197 as the catalytic nucleophile (*22*). Glu233 and Asp300 are hydrogen-bonded to each other, via an intervening water molecule (W555), as well as to the nitrogen atom of the nonhydrolyzable *N*-glycosidic bond in the acarbose−PPA complex. As we proposed (*16*), Glu233 (very close to the chloride ion) is the most appropriate candidate for the role of the catalytic acid/base. A scheme of the reaction sequence at the catalytic center is presented in Figure 2.

X-ray structural analyses of the interaction between the pseudo-tetrasaccharide acarbose and the mammalian α-amylases showed that a ligand longer than the initial molecule remained bound to the active site. Because one glycosidic bond of the acarbose molecule may be hydrolyzed by the mammalian α-amylase, yielding truncated acarbose molecules (pseudo-trisaccharide) as well as glucose, the case for transglycosylation was examined (*16, 17, 19*). Extended species have been seen in other family 13 glycoside hydrolase complexes (*23*−*25*). These results led to debate about the occurrence of either "bi-reaction" mechanisms (condensation or transglycosilation) or overlapping networks of oligosaccharides. For the α-amylase family, the discussion was still open and whether "bi-reaction" occurs in the crystal remained as yet unproven.

Our current study, which analyzes the interaction between PPA and K2 (truncated acarbose), provides experimental evidence that the mammalian α-amylases are able to catalyze further reactions on the pseudo-trisaccharide product.

MATERIALS AND METHODS

Crystals of PPA were grown at 4 °C as in our previous studies (*14*). The active center of PPA is not blocked in the crystal packing and can be easily accessed by external ligands. This allowed us to obtain enzyme−inhibitor complexes by soaking native crystals in buffered crystal-stabilizing solutions of the compound of interest. The two complexes described in the present study were formed by soaking crystals of PPA in a solution containing 1 mM K2 in 10 mM Tris (pH 8), 1 mM $CaCl_2$, 2 M NaCl, for 24 h at room temperature and 4 °C, respectively. The K2 soaking experiments were performed at the same concentration as previously used with the acarbose compound (*16*). Maximal enzymatic activity occurs around pH 7, and the enzyme is still highly active at pH 8. (*26, 27*). Crystals of the complexed PPA were isomorphous to those obtained with the free enzyme.

X-ray data to 1.38 Å (Table 1) were collected from a single crystal grown at 4 °C and soaked at room temperature, on the ESRF ID14-2 beam line ($\lambda = 0.933$ Å), in Grenoble, at 100 K. X-ray data to 2.3 Å (Table 1) were collected from a single crystal (grown and soaked at 4 °C) frozen to 100 K for data collection using a Mar-Research Imaging plate scanner as detector and a rotating anode as X-ray source. Data processing and reduction were carried out with the HKL program suite (*28*).

[1] Abbreviations: PPA, pig pancreatic α-amylase; HPA, human pancreatic α-amylase; BSUA, *Bacillus subtilis* α-amylase; TAKA-amylase, *Aspergillus orizae* α-amylase; K2, acarviosine-glucose (truncated acarbose) molecule; ACA, acarbose; G5, maltopentaose.

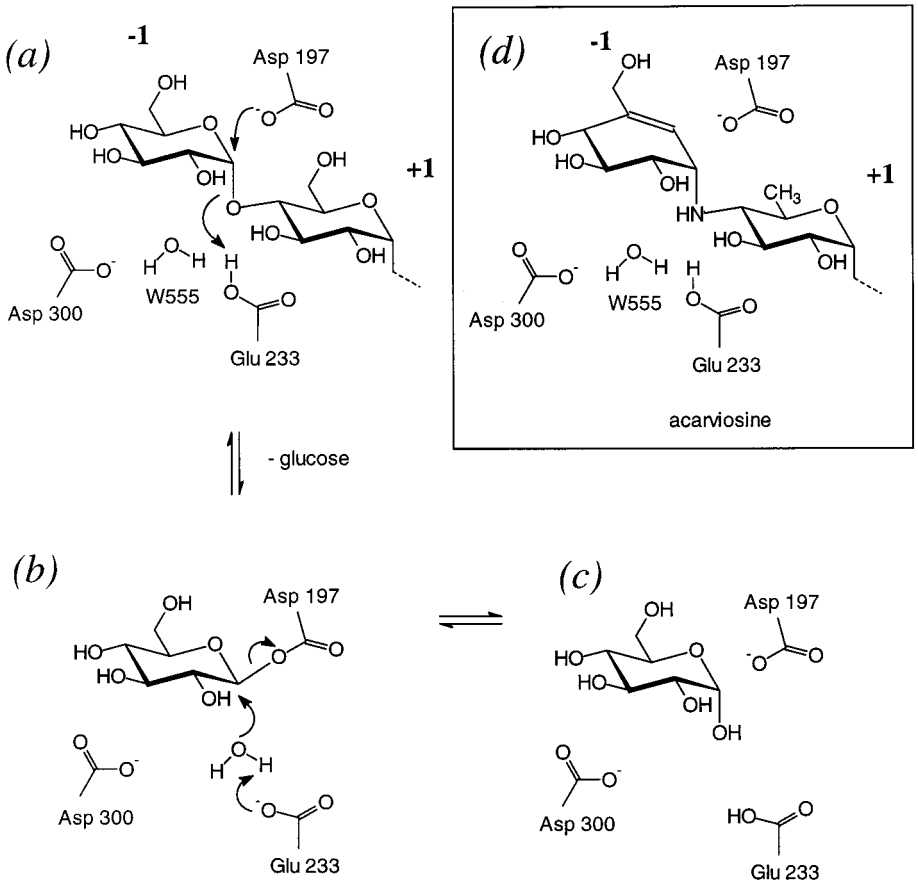

FIGURE 2: Proposed reaction mechanism for α-amylases viewed at subsites −1 and +1. (a) The nucleophile, unambiguously identified by McCarter and Withers (*22*) as Asp197, attacks the anomeric carbon with concomitant protonation of the glycosidic oxygen by Glu233, widely regarded as a general acid/base catalyst. (b) The resulting covalent *β*-glycosyl-enzyme intermediate is hydrolyzed by a water molecule activated by the deprotonated Glu233. (c) The final product with retained anomeric configuration. The role of Asp300 is not known, but its sequence conservation and its position suggest that it may be essential for regulating the pK_a of the general acid/base during catalysis cycles. Such a pK_a cycling of the general acid/base has been demonstrated for a retaining xylanase (*39*). (d) Binding of the acarviosine moiety in the acarbose-derived extended ligand (*16*).

Table 1: Data Collection Statistics

	PPA/K2 complexes	
	soaking at 20 °C[a]	soaking at 4 °C[b]
space group	$P2_12_12_1$	$P2_12_12_1$
a (Å)	69.28	69.57
b (Å)	113.55	113.23
c (Å)	117.16	117.03
resolution of data	35−1.38	35−2.35
(outer shell) (Å)	(1.42−1.38)	(2.40−2.35)
no. of measurements	507677	125237
no. of unique reflections	184003	38657
R_{merge}[c] (outer shell)	0.067 (0.451)	0.146 (0.487)
multiplicity	2.8 (2.3)	3.1 (2.9)
$\langle I/\sigma I\rangle$ (outer shell)	13.10 (2.50)	7.0 (5.0)
completeness (outer shell) (%)	97.04 (96.13)	98.6 (96.3)

[a] X-ray source was the ESRF beamline ID14-2 Grenoble. [b] X-ray source was the rotating anode with Mar-Research plate scanner. [c] $R_{merge} = \sum_h\sum_i|I_{h,i} - \langle I_h\rangle|/\sum_h\sum_i|I_{h,i}|$.

Refinement of the High-Resolution Model. Simulated annealing was first performed with CNS (*29*) using the data recorded between 35 and 1.38 Å with a standard approach. The behavior of the free *R*-factor was monitored; of the reflection data, 1.6% was set aside for the test set. No oligosaccharide atoms were included in the model until the refinement of the protein had reached convergence. It is worth noting that the initial difference electron density maps showed well-defined continuous density for the sugar moieties in six subsites of the active site depression, from −4 to +2 (nomenclature according to ref *30*). The introduction of a single hexasaccharide species bound to the active site appeared consistent with the subsequent refinement procedure.

Once refinement with CNS had converged, the *R*-factor and R_{free} were 0.188 and 0.197, respectively; as these values were rather high and because of the occurrence of appreciable F_o-F_c electron density peaks on almost every atom, an anisotropic refinement with the program SHELX-97 (*31*) was deemed necessary.

The model was treated isotropically for a few cycles; subsequently, anisotropic treatment was introduced. The R_{free} factor was monitored to calibrate restraints and weights and to establish whether this approach was justified. Each refinement macrocycle in general consisted of 8 cycles of automatic minimization using the conjugate gradient least-squares refinement option followed by σ_A-weighted $2F_o-F_c$ and F_o-F_c map calculation and manual rebuilding. Rigid-bond restraint and "similarity restraints" were applied to the atomic displacement parameters of protein atoms, and an approximately isotropic behavior was imposed on solvent atoms.

Restrained anisotropic thermal parameters were first introduced for Ca^{2+}, Cl^-, and S atoms; the resulting F_o-F_c

Table 2: Refinement and Structure Quality Statistics for the PPA/K2 Complexes

	soaking at 20 °C	soaking at 4 °C
resolution used in refinement (Å) (outer shell)	35−1.38 (1.42−1.38)	35−2.35 (2.40−2.35)
data/parameters (in final cycles of SHELX)	184003/47628	
no. of protein atoms	4177[b]	3937[b]
discretely disordered residues	48	8
no. of water molecules (full/half occupancy)	551/208 (B < 50 Å^2)	577 (B < 50 Å^2)
no. of ligand atoms	89	88
no. of ethylene glycol atoms	52	16
no. of ion atoms	5 (1 Ca^{2+}, 4 Cl^-)	4 (1 Ca^{2+}, 3 Cl^-)
R_{cryst}[a] (outer shell)	12.51 (22.6)	18.06 (21.50)
R_{free} (outer shell)	15.35 (24.4)	22.22 (23.27)
R_{cryst} for all data	12.53	18.96
mean protein atoms B (Å^2)	19.00	15.24
mean main-chain atoms B (Å^2)	16.97	15.14
mean side-chain B (Å^2)	20.70	19.30
mean solvent atom B (Å^2)	35.73	26.92
mean ligand atoms B (Å^2) (active site)	29.00	40.17
subsite: −4, −3, −2	48.92, 24.15, 20.71	49.90, 35.03, 29.25
subsite: −1, +1, +2	24.41, 25.26, 29.63	38.38, 48.76
mean ligand atoms B (Å^2) (surface site)	46.05	42.90
B value (Wilson plot) (Å^2)	15.86	12.96
rms deviation of 1−2 bonds (Å)	0.013	0.016
rms deviation of 1−3 bonds (Å)/angles (deg)	0.030 Å	1.46°
rms deviation of chiral volumes (Å^3)/impropers (deg)	0.074 Å^3	1.04°

[a] R_{cryst} is defined as $\sum|F_o - F_c|/\sum|F_o|$. [b] This apparent discrepancy results from different modeling of alternative conformations in the two structures.

Fourier difference map showed the existence of alternate conformations for S atoms of residues Cys70, Cys115, Cys141, and Cys450 involved in disulfide bridges. In the refinement procedure, cysteine and cystine residues were refined with their occupancies coupled in complementary fashion. In the subsequent stages, the restrained anisotropic thermal parameters for all non-H atoms were introduced. In the refinement procedure, bonding distances for the K2 ligand were restrained to target values derived from our crystal structure of the acarbose-complexed PPA (*16*).

The high-quality electron density maps resulting from restrained anisotropic refinement allowed modeling of discrete disorder in the enzyme model. Further water molecules were added to the model; a number of solvent molecules were refined with occupancy of 0.5 (see Table 2). Electron density for ethylene glycol molecules originating from the cryo-protectant was visible, and the molecules were added to the model. Hydrogen atom positions were generated automatically by adopting geometric criteria and refined using a "riding" model. The isotropic atomic displacement parameters for hydrogen atoms were made dependent on the equivalent isotropic displacement parameters of the atoms to which they were attached. The drop in both R-factor and R_{free} by 6% and 4%, respectively, unambiguously demonstrated that the anisotropic refinement was meaningful. The quality of the maps was also substantially improved. A last conjugate gradient least-squares refinement cycle was carried out against all data, including the test data set. To obtain the estimated standard deviations in the atomic parameters, a final cycle of overlapped block-matrix (BM) least-squares refinement was carried out, in which the restraints were turned off. Coordinates of the high-resolution model of the pig pancreatic α-amylase have been deposited with the Brookhaven Protein Data bank (*32*) (accession code 1HXO).

Refinement of the Low Temperature Complex. As in the previous structure, simulated annealing was performed with CNS following the same protocol. Even with the starting phases, clear continuous density corresponding only to the initial inhibitor structure (three units) was observed in the binding cleft (subsites −4, −3, −2). Nevertheless, the electron density maps (with σ_A-weighting) calculated before the incorporation of any sugar moiety were carefully examined.

The structure quality statistics for each structure determination are described in Table 2. The surface site ligand (Table 2) corresponds to a short oligosaccharide bridging two enzyme molecules related by a symmetry operator as previously observed (*19*, *33*).

Mass Spectrometry. Enzyme-catalyzed incorporation of ^{18}O into the K2 molecule using $H_2{}^{18}O$ was analyzed by MALDI-TOF mass spectrometry. The mass spectra collected included the calculated K2 spectrum and spectra obtained when K2 was incubated with $H_2{}^{18}O$ alone and $H_2{}^{18}O$ plus PPA, respectively (see Mass Spectrometry under Results and Discussion). The mixture with $H_2{}^{18}O$ was composed of 9 μL of $H_2{}^{18}O$, 0.5 μL of K2 solubilized in water (10 mg/mL), and 0.5 μL of the PPA buffer (Tris-HCl, 10 mM; $CaCl_2$, 1 mM; NaCl, 10 mM). An enzyme concentration of 15 mg/mL was used in the experiments. One microliter of sample was mixed with 1 μL of 2.5-dihydrobenzoic acid matrix (DHB, Sigma); 1 μL of the resulting mixture was deposited on a matrix-assisted laser desorption ionization time-of-flight (MALDI-TOF) sample plate. The mixture was allowed to dry at room temperature and analyzed in the positive reflectron mode using a voyager DE-RP MALDI-TOF instrument (Perspective Biosystem Inc., Framingham, MA). The spectra shown represent the average of 256 laser shots. Acquisition conditions were as follows: accelerating voltage, 20 kV; grid voltage, 59%; guide-wire voltage, 0.15%; extraction delay, 50 ns (no mass gate). Each spectrum was internally calibrated using ions 137,0239 and 273,0399 with respect to the matrix.

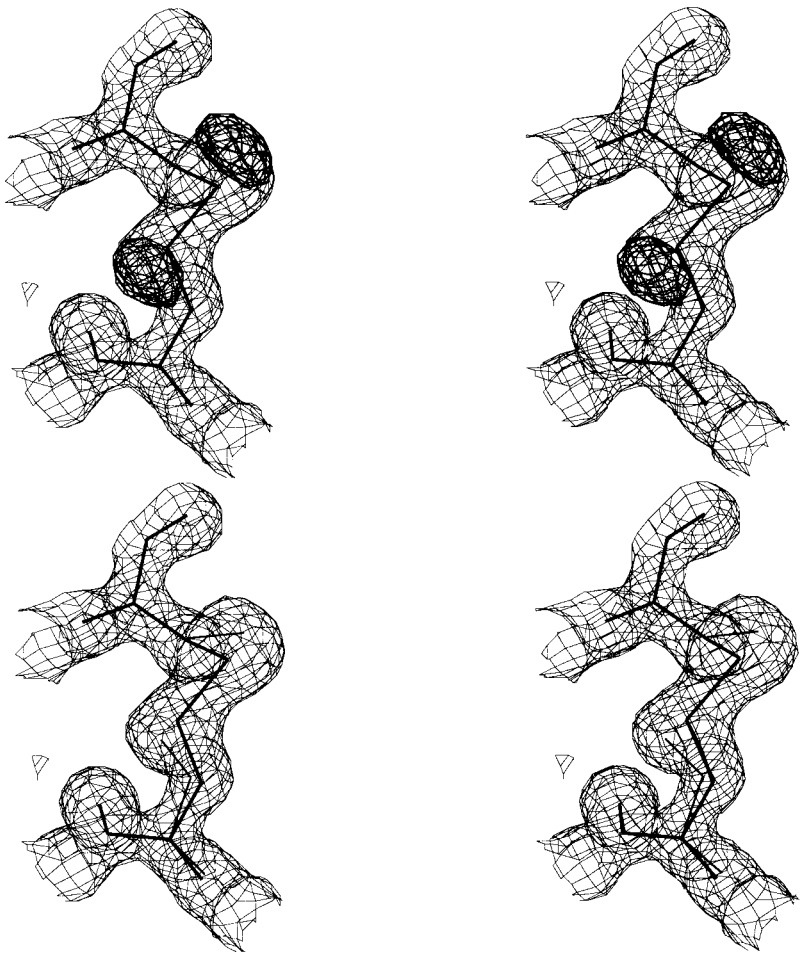

FIGURE 3: Electron density maps for the disulfide bridge between Cys70 and Cys115. The $2F_o-F_c$ electron density map generated with final phases is contoured at 0.5×10^{-3} Å. Alternate conformations of the Sγ atoms have been omitted for calculation of the F_o-F_c difference Fourier map; the positive electron density peaks (contoured at 0.12×10^{-3} Å) are shown (darker lines). The final refined coordinates (with opening of the bridge; thinnest lines) are shown.

RESULTS AND DISCUSSION

High-Resolution Model of the Pancreatic α*-Amylase.* The model, refined at high resolution, clearly showed the presence of alternate side-chain conformations for 48 residues out of 496. Most of them are located on the surface of the protein, and two (Glu240 and Ser311) are in the active site area. Three loop regions showed alternate conformations. Two of the three, loops 237−241 and 303−311, facing each other, constitute the surface edge of the active site toward the solvent. The mobility of these regions suggests that they take part in the particular processive mechanism of mammalian α-amylases. The third loop (134−141) is located at the top of domain B. The three loop regions observed here in alternate conformation are elements of the flexibility of the enzyme capable to move in response to inhibitor binding (*16, 17, 19, 34*).

Disulfide Bridges. With atomic resolution data, we were able to look in detail at disulfide bridges of the pancreatic α-amylase. Alternate conformations of the Sγ atoms were observed for cysteine residues 70, 115, 141, and 450 (involved in three disulfide bridges: 70−115, 141−160, and 450−462). These structural changes most probably arose from radiation damage whose effects have been discussed and reported (see ref *35*). Negative electron density peaks (about -9.5σ) at the position of the disulfide bridges accompanied by positive electron density peaks (about $+10.4\sigma$) in proximity were observed. An example is shown in Figure 3 with the disulfide bridge between Cys70 and Cys115, in which both cysteine residues display alternate conformations. All the disulfide bridges that have been modified were partially exposed to the solvent.

Chloride Ions. In the mammalian pancreatic α-amylases, a chloride ion was identified bound in close proximity to the active site and involved in a network of interactions with the catalytic residues (*16*). The chloride ion acts as an activating effector of the pancreatic α-amylase (*13*). In the course of analyzing the water structure, we discovered three sites showing a strong well-defined F_o-F_c electron density. A water molecule was not sufficient to account for the observed density, and the stereochemistry of the site was indicative of chloride ions, with average hydrogen bonding distances of about 3.2 Å. The introduction of these chloride ions appeared consistent with the subsequent refinement procedure with no further F_o-F_c Fourier difference present. *B*-factor values for the ions ranged from 18 to 25 Å^2 and were of a magnitude similar to those of the protein atoms involved in the interaction. All the chloride ions are found in the vicinity of the active site (Figure 4).

Active Site Ligand Structure. Condensation Mechanism. The initial difference electron density map calculated from

FIGURE 4: Stereo Molscript (*40*) diagram showing the relative positioning of the active site (the hexasaccharide ligand is shown), together with the chloride (4 spheres) and calcium (1 sphere) ions. The central Cl^- ion (*13*) is bound within the carboxyl end of the β-barrel, in close proximity to the catalytic center.

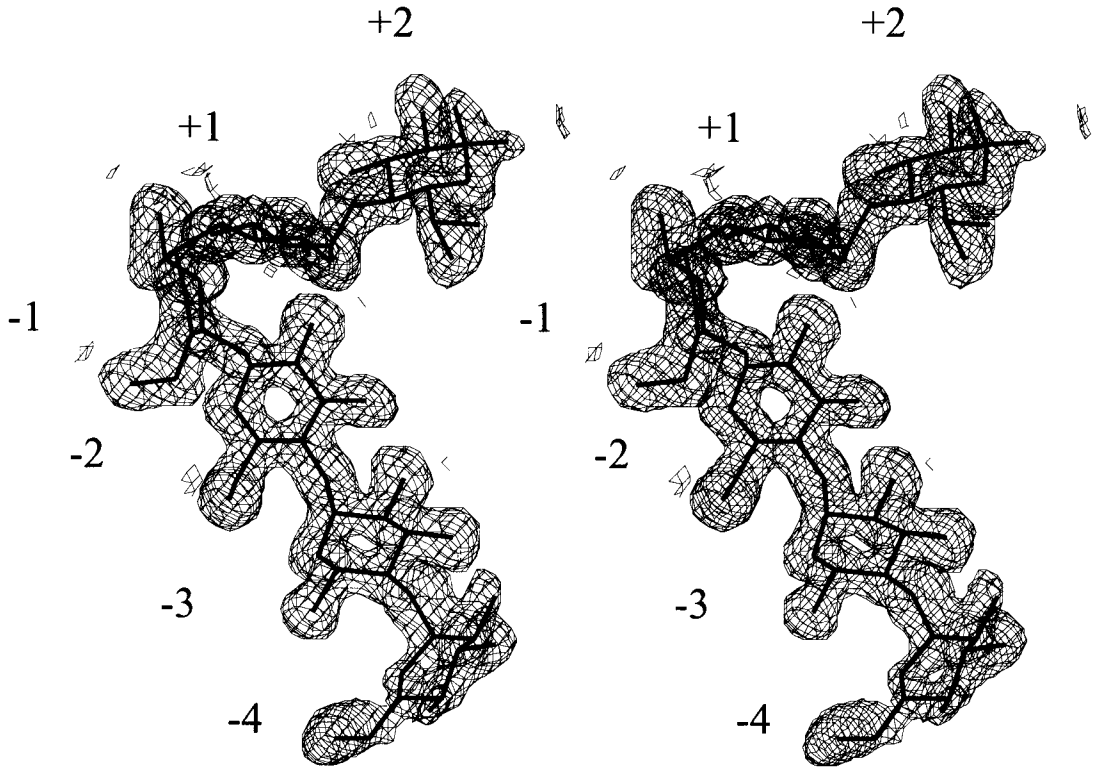

FIGURE 5: Stereo electron density for the final hexasaccharide ligand bound to the −4 to +2 subsites of the enzyme. The map shown is a σA-weighted $2F_o-F_c$ electron density contoured at 0.5×10^{-3} Å. The figure was prepared using TURBO−FRODO (*41*).

the high-resolution model (crystals soaked overnight in K2 solution at room temperature) showed a continuous electron density corresponding to a hexasaccharide species occupying the active site from subsite −4 to subsite +2. The incorporation of a single hexasaccharide appeared consistent with the subsequent refinement procedure performed using CNS, and this was reminiscent of previous results obtained with acarbose (*16*, *19*). However, after convergence of the refinement procedure, positive electron density peaks occurred in the F_o-F_c difference electron density map in several parts of the ligand. Most of them were found in catalytic subsite −1 and on the scissile bond (linkage between subsites −1 and +1). As explained under Materials and Methods, an anisotropic description of the atomic displacement with the program SHELX-97 (*31*) was deemed necessary for the ligand structure.

The quality of the resulting electron density maps demonstrated that the anisotropic refinement was meaningful. The resulting electron density of the α-1,4-linkages between all six sugar units was well-defined. Two 6-deoxy units,

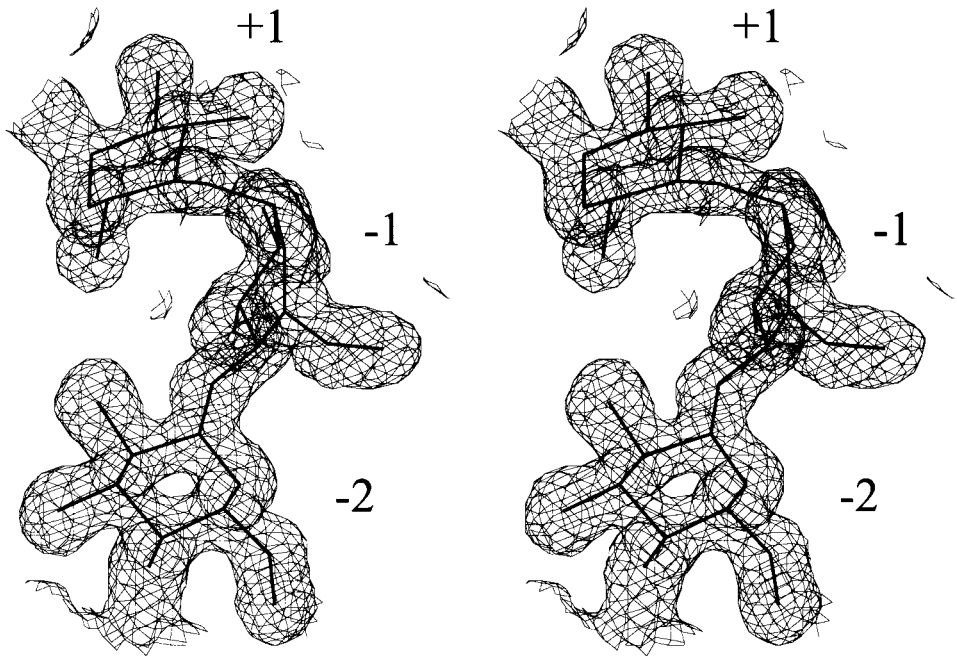

FIGURE 6: Close-up view showing the $2F_o-F_c$ electron density (1.6σ contoured) around the newly formed $-2/-1$ glycosidic linkage between the two K2 molecules. The acarviosine moiety of the K2 molecule at the top is bound with its cyclitol unit and 4,6-dideoxy-4-amino-D-glucose at subsites -1 and $+1$. The glucose ring of the K2 molecule, at the bottom, is bound to subsite -2.

Table 3: Torsion Angles around the Glycosidic Bonds and O2−O3′ Hydrogen Bond Distances

	φ (O5−C1−O4′−C4′) (deg)				ψ (C1−O4′−C4′−C5′) (deg)				O2−O3′(Å)			
glycosidic	PPA/K2[a]		PPA/ACA[b]	BSUA/G5[c]	PPA/K2[a]		PPA/ACA[b]	BSUA/G5[c]	PPA/K2[a]		PPA/ACA[b]	BSUA/G5[c]
linkage	20 °C[a]	4 °C[a]	20 °C		20 °C	4 °C	20 °C		20 °C	4 °C	20 °C	
−4/−3	91.99	126.74			−120.37	−174.35			#[d]	2.53		
−3/−2	123.40	115.30	116.16	127.2	−110.11	−109.74	−107.01	−107.2	2.72	2.73	2.72	2.7
−2/−1	89.36	75.13	89.89	86.0	−156.20	−143.98	−150.12	−153.7	#	#	#	#
−1/+1	30.02	15.47	17.82	25.5	−141.95	−145.51	−149.11	−148.6	#	#	#	#
+1/+2	115.37		113.50	109.7	−116.06		−99.52	−116.8	2.58		2.84	2.7

[a] Present structures, soaking conditions. [b] (*15*), PDB File Name 1PPI. [c] (*32*), PDB File Name 1BAG. [d] #, no hydrogen bond.

bound to subsites -3 and $+1$, were identified (unambiguously supported by the very well resolved electron density maps; see Figure 5). Electron density corresponding to the glucose residue bound to subsite $+2$ allowed modeling of the pyranoside ring in which the O6 atom had an alternate conformation; the density at this subsite revealed that the O1 hydroxyl on the anomeric carbon was present as a mixture of both anomers as a result of mutarotation with the α-anomer present with an occupancy of about 0.74 and the β-anomer 0.26. The electron density maps at subsite -1 obviously accommodated the $^2H_3$ half-chair conformation of the cyclitol moiety. Given the quality of the whole electron density maps which allow an accurate description at the atomic level of the model, the structure of the hexasaccharide could be defined as composed of two α-1,4-linked K2 molecules; a close-up view of the newly formed glycosidic bond is shown in Figure 6. The glycosidic bond torsion angles and hydrogen bonds of the ligand are detailed in Table 3. The similarity between the torsion angles obtained in the present model and those observed in an intact maltopentaose bound to *Bacillus subtilis* α-amylase (*36*) is shown. Particularly interesting are the torsion angles, around the glycosidic bond $-2/-1$, which characterize the newly formed glycosidic bond between the two α-1,4-linked K2 molecules. In both structures, these values are almost identical, which is consistent with the proposed structure; it should be noted that a same value was also observed in the ACA/PPA ligand (*16*). The cyclitol unit bound to subsite -1 is clearly distorted toward a $^2H_3$ half-chair with a torsion angle C2−C1−O5−C5 of 13° (in the cyclitol unit, O5 is replaced by a carbon linked by a double bond to C5). This planarity resembles the planarity that exists in the transition state. This torsion angle is −62° in the sugar ring bound to subsite $+2$; it shows similar values in sugar rings bound to subsites -3, -2, and $+1$; this torsion angle is −63° in the $^4C_1$ chair minimum energy conformation (*37*).

In addition, to test the validity of our model, a refinement of the individual crystallographic occupancies of sugar units was performed without imposing any restraints. From the nonreducing end of the ligand (subsite -4) to the reducing end (subsite $+2$), the occupancies refined to the following values: 0.82, 0.95, 0.97, 0.90, 0.95, 0.91, which confirm that the observed hexasaccharide is mainly composed of a genuine single species and not of an overlap of K2 molecules.

After modeling the carbohydrate moieties, the protein, and the solvent and location of hydrogen atoms, refinement converged to an *R*-factor of 12.51% and an R_{free} of 15.3%. Final refinement against all reflections, including those previoulsy set aside for R_{free} calculation, resulted in an *R*-factor of 12.53%, and the largest peak and hole in the difference Fourier synthesis correspond to 0.28, -0.21×10^{-3} Å, respectively.

Structure analysis at the atomic level unambiguously points to the presence of a hexasaccharide species composed of two α-1,4-linked original molecules bound to the active site of the enzyme. This is important because it implies that an enzyme-catalyzed condensation occurred in the crystal to give a hexasaccharide product.

Mass Spectrometry. A prerequisite to any enzymatic condensation event generating a hexasaccharide species from K2 is the formation of a competent glycosyl-enzyme intermediate from K2, which can lead to either condensation or regeneration of K2. Using $H_2{}^{18}O$ as a probe, we have tried to find evidence for the generation of a K2-based glycosyl-enzyme with PPA. If PPA was indeed able to reach the glycosyl-enzyme intermediate stage with K2, then incubation with $H_2{}^{18}O$ would yield a higher incorporation of ^{18}O in the presence of PPA than in a control experiment without enzyme.

The calculated mass spectrum of K2 (Figure 7A) showed one peak at the *m*/*z* value of 506.18 Da corresponding to the theoretical mass of $K2+Na^+$, i.e., 506.184 Da. When K2 was incubated in $H_2{}^{18}O$ alone for 19 h, a slight increase of the intensity was noticed at $m/z = 508.15$ indicative of a weak spontaneous exchange of ^{16}O by ^{18}O (Figure 7B). When PPA was added to the mixture, a significant increase of the intensity of this peak was observed (Figure 7C). The reaction diagram shown in Figure 8A illustrates the incorporation of ^{18}O into K2 according to the mechanism widely proposed for retaining α-glucosidases. In such a reaction, the enzyme attacks the C1−O1 bond of the reducing glucose ring, giving rise to the glycosyl-enzyme intermediate. The incoming solvent molecule ($H_2{}^{18}O$) then acts as the nucleophile in the breakdown of the intermediate, resulting in the formation of a product in which ^{18}O is incorporated into the reducing end of the K2 molecule. As a consequence, PPA appears to be able to "turn-over" K2 and, therefore, to reach the glycosyl-enzyme intermediate stage necessary for the condensation reaction.

In the crystal, a similar reaction may take place with the initial K2 molecules bound in the −3, −2, and −1 subsites (see Figure 8B). As an alternate nucleophile, a K2 molecule can probably attack the glycosyl-enzyme intermediate and produce a pseudo-hexasaccharide species by condensation. Probably after a translation in the active site, the condensation product accumulates in the crystal, bound to subsites −4 to +2 in a nonproductive mode. This condensation product can only accumulate after a migration in the active site in order to escape rehydrolysis. Such a migration has also been mentioned with TAKA-amylase/acarbose complexes (*24*). The inhibitory properties of compounds made like that produced by the condensation reaction have been measured and found to be approximately 100 times better than that of K2 (*6*). This very large increase in affinity probably explains the accumulation (according to the subsite affinity profile) of condensed products in the crystal.

Whether an extended species as observed in the crystal may be released in the medium remains unproven. Our attempts to find evidence for the condensation product in redissolved crystals have failed.

Low Temperature Complex. The hydrolytic activity of PPA is strongly reduced at low temperature (*38*), and it is likely that the same reduction occurs for the condensation reaction. Accordingly, an experiment was designed in which the crystal was kept at low temperature throughout the entire experiment. Crystals were grown and soaked at 4 °C (for 24 h) and frozen for X-ray data collection (see Materials and Methods and Table 1). In such conditions, the accumulation of the hexasaccharide species was not observed. The results show strong binding of the K2 molecules at the entrance of the active site cleft (subsites −4, −3, −2). No sugar density could be detected in subsite +2; a weak

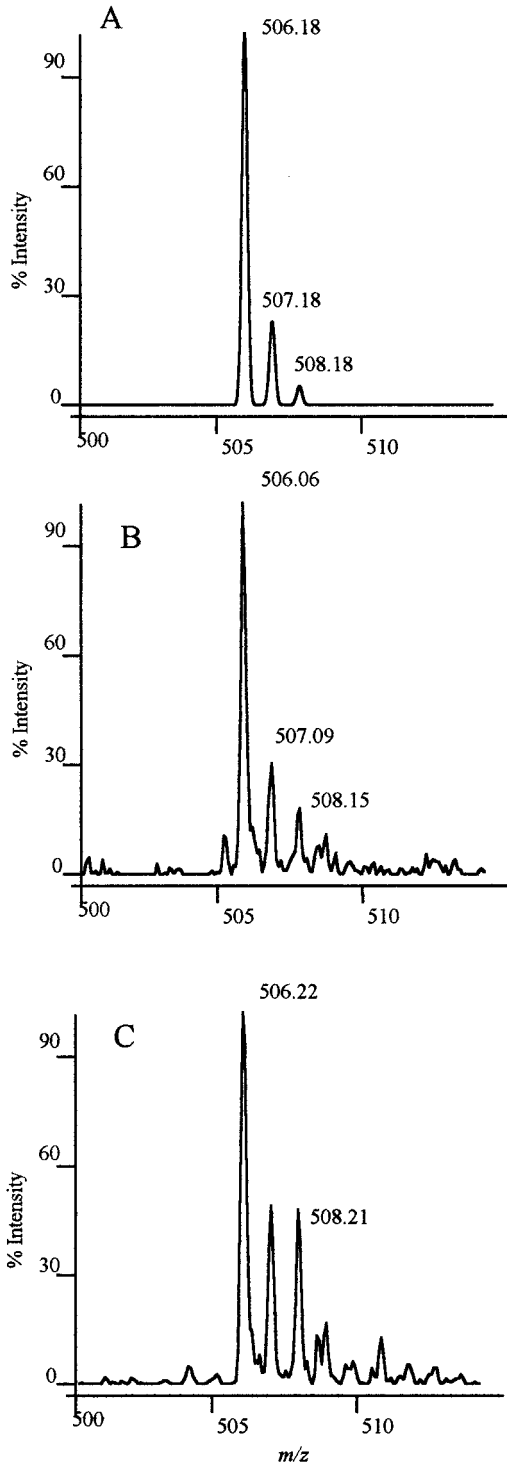

FIGURE 7: Mass spectra showing the relative intensity of the peak corresponding to the incorporation of ^{18}O in K2. (A) Calculated spectrum showing the isotopic profile of the starting K2 compound. (B) MALDI spectrum when K2 has been incubated in $H_2{}^{18}O$ alone. (C) MALDI spectrum when K2 has been incubated in $H_2{}^{18}O$ with PPA.

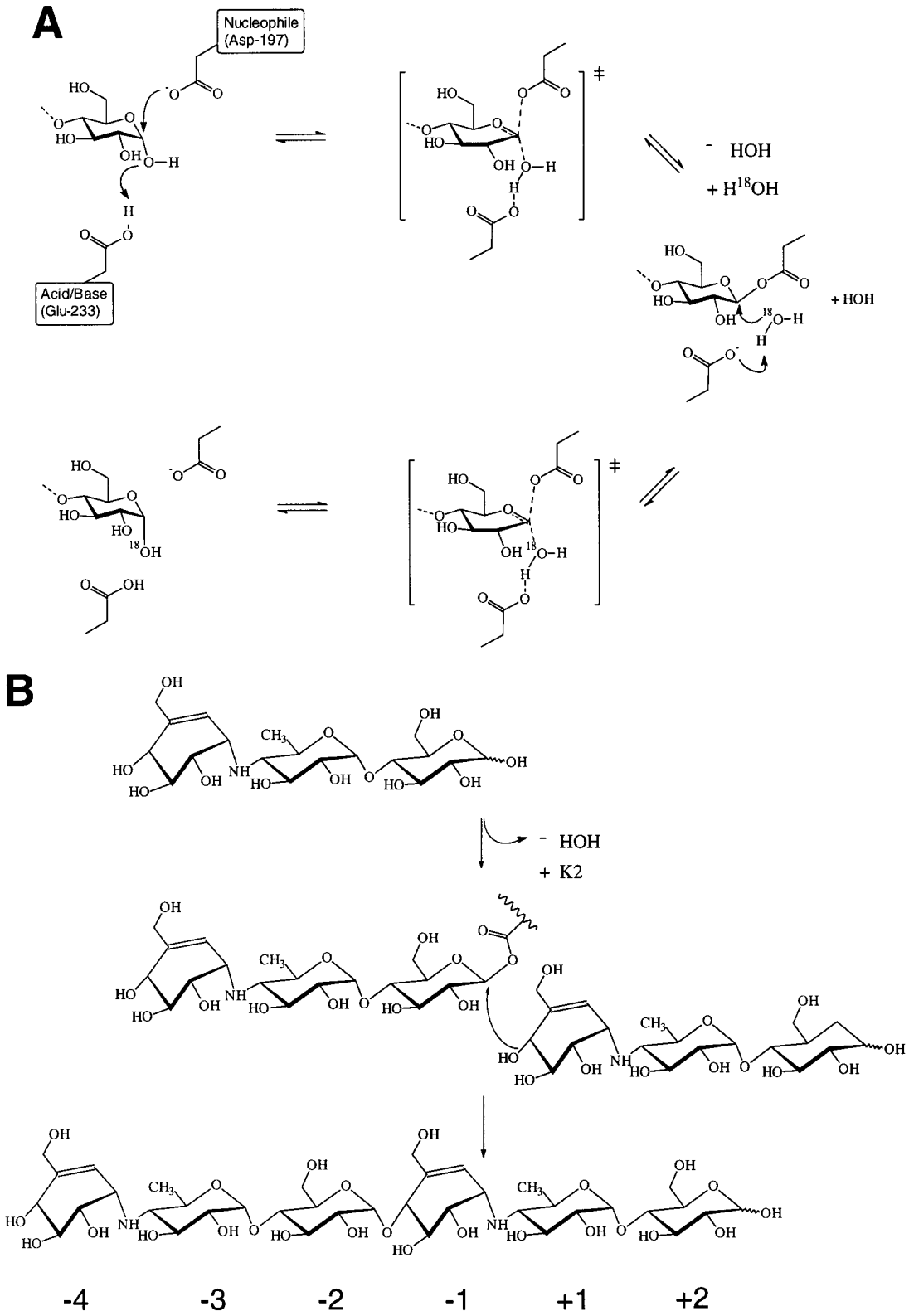

FIGURE 8: Schematic figure showing a possible bimolecular mechanism for the formation of the pseudo-hexasaccharide species observed in the active site. (A) Incorporation of ^{18}O from $H_2{}^{18}O$. (B) Condensation reaction of two molecules of K2.

discontinuous electron density was observed in subsites −1 and +1; no carbohydrate could be modeled in these subsites. Given the low catalytic activity of the enzyme at low temperature, the K2 molecule probably did not undergo serious turnover. Only unproductive binding of the molecule (subsites −4 to −2) occurred and dominated the binding scheme (under these unfavorable conditions of temperature). It seems clear that accumulation of an extended species longer than the initial molecule in the active site of PPA does not occur when the reaction has been carried out under unfavorable conditions. This again is in favor of an enzyme-catalyzed reaction.

The present results have to be related to previous results obtained upon incubation of PPA with acarbose (*16*, *19*),

because K2 is the product obtained when acarbose is hydrolyzed by α-amylase (*8*). With both molecules, the same pseudo-trisaccharide structure is observed bound to subsites −1, +1, +2, identically linked to a glucose residue bound to subsite −2; torsion angles around the glycosidic bond −2/−1 are very similar (see here above and Table 3). Taken together, our data and observations strengthen the proposal of Nahoum et al. (*17*) that upon interaction with pancreatic α-amylase, acarbose undergoes a transglycosylation, a reaction similar, after cleavage of the glucose residue at its reducing end, to the condensation reaction of K2.

The present study provides clear evidence that the condensation reaction does occur in the crystal and sheds light on the main rules underlying the inhibition mechanism of α-amylase by the trestatin-derived inhibitors. Our results show that the structure of the species bound to the active site is similar to that of the higher homologues in the trestatin family providing the strongest inhibition of α-amylase.

ACKNOWLEDGMENT

We are grateful to Dr. Gerlind Sulzenbacher for useful discussions and critical reading of the manuscript. We thank Dr. Kieron Brown for assistance in the Synchrotron data collection and critical reading of the manuscript. We thank Bayer-Pharma, Puteaux, France, for support.

REFERENCES

1. Henrissat, B. (1991) *Biochem. J. 280*, 309−316.
2. Coutinho, P. M., and Henrissat, B. (1999) in *Recent Advances in Carbohydrate Bioengineering* (Gilbert, H. J., Davies, G. J., Henrissat, B., and Svensson, B., Eds.) pp 3−12, The Royal Society, Cambridge, U.K.
3. Puls, W., Keup, U., Krause, H. P., Thomas, G., and Hoffmeister, F. (1977) *Naturwissenschaften 64*, 536−537.
4. Schmidt, D. D., Frommer, B., Junge, L., Müller, W., Wingender, W., and Truscheit, E. (1977) *Naturwissenschaften 64*, 535−536.
5. Bischoff, H. (1994) *Eur. J. Clin. Invest. 24*, 3−10.
6. Schmidt, D. D., Frommer, B., Junge, L., Müller, W., Wingender, W., and Truscheit, E. (1981) in *First international symposium on acarbose* (Creutzfeldt, E. W., Ed.) pp 5−15, Excerpta Medica, Amsterdam.
7. Junge, B., Böshagen, H., Stoltefuss, J., and Muller, L. (1980) in *Enzyme Inhibitors* (Brodbeck, U., Ed.) pp 123−137, Verlag Chemie, Weinheim.
8. Müller, L., Junge, B., Rauenbusch, E., Frommer, W., Schmidt, D., and Truscheit, E. (1981) in *First international symposium on acarbose* (Creutzfeldt, E. W., Ed.) pp 142−146, Excerpta Medica, Amsterdam.
9. Wilcox, E. R., and Whitaker, R. J. (1984) *Biochemistry 23*, 1783−1791.
10. Robyt, J. F., and French, D. (1970) *J. Biol. Chem. 245*, 3917−3927.
11. Steer, M., and Levitzki, A. (1973) *FEBS Lett. 31*, 89−92.
12. Vallee, B. L., Stein, E. A., Summerwell, W. N., and Fisher, E. H. (1959) *J. Biol. Chem. 234*, 2901−2929.
13. Levitzki, A., and Steer, M. L. (1974) *Eur. J. Biochem. 41*, 171−180.
14. Qian, M., Haser, R., and Payan, F. (1993) *J. Mol. Biol. 231*, 785−799.
15. Brayer, G. D., Luo, Y., and Withers, S. G. (1995) *Protein Sci. 4*, 1730−1742.
16. Qian, M., Buisson, G., Duée, E., Haser, R., and Payan, F. (1994) *Biochemistry 33*, 6284−6294.
17. Nahoum, V., Roux, G., Anton, V., Rougé, P., Puigserver, A., Bischoff, H., Henrissat, B., and Payan, F. (2000) *Biochem. J. 346*, 201−208.
18. Brayer, G. D., Sidhu, G., Maurus, R., Rydberg, E. H., Braun, C., Wang, Y., Nguyen, N. T., Overall, C. M., and Withers, S. G. (2000) *Biochemistry 39*, 4778−4791.
19. Gilles, C., Astier, J. P., Marchis-Mouren, G., Cambillau, C., and Payan, F. (1996) *Eur. J. Biochem. 238*, 561−569.
20. Koshland, D. E. (1953) *Biol. Rev. 28*, 416−436.
21. McCarter, J. D., and Withers, S. G. (1994) *Curr. Opin. Struct. Biol. 4*, 885−892.
22. McCarter, J. D., and Withers, S. G. (1996) *J. Biol. Chem. 271*, 6889−6894.
23. Strokopytov, B., Knegtel, R. M. A., Penninga, D., Rozeboom, H. J., Kalk, K. H., Dijkhuizen, L., and Dijkstra, B. W. (1996) *Biochemistry 35*, 4241−4249.
24. Brzozowski, A. M., and Davies, G. J. (1997) *Biochemistry 36*, 10837−10845.
25. Dauter, Z., Dauter, M., Brzozowski, A. M., Christensen, S., Borchert, T. V., Beier, L., Wilson, K. S., and Davies, G. J. (1999) *Biochemistry 38*, 8385−8392.
26. Wakim, J., Robinson M., and Thoma, J. A. (1969) *Carbohydr. Res. 10*, 487−503.
27. Ishikawa, K., Matsui, I., Kobayashi, S., Nakatani, H., and Honda, K. (1993) *Biochemistry 32*, 6259−6265.
28. Otwinowski, Z., and Minor, W. (1997) in *Methods in Enzymology: Macromolecular Crystallography, Part A* (Carter, C. W., Jr., and Sweet, R. M., Eds.) pp 307−326, Academic Press, London and New York.
29. Brünger, A. T., Adams, P. D., Clore, G. M., DeLano, W. L., Gros, P., Grosse-Kunstleve, R. W., Jiang, J. S., Kuszewski, J., Nilges, M., Pannu, N. S., Read, R. J., Rice, L. M., Simonson, T., and Warren, G. L. (1998) *Acta Crystallogr. D54*, 905−921.
30. Davies, G. J., Wilson, K. S., and Henrissat, B. (1997) *Biochem. J. 321*, 557−559.
31. Sheldrick, G. M., and Schneider, T. R. (1997) *Methods Enzymol. 277*, 319−343.
32. Bernstein, F. C., Koetzle, T. F., Williams, G. J. B., Meyer, E. T., Jr., Brice, M. D., Rodgers, J. R., Kennard, O., Shimanouchi, T., and Tasumi, M. (1977) *J. Mol. Biol. 112*, 535−542.
33. Larson, S. B., Greenwood, A., Cascio, D., Day, J., and McPherson, A. (1994) *J. Mol. Biol. 235*, 1560−1584.
34. Bompard-Gilles, C., Rousseau, P., Rougé, P., and Payan, F. (1996) *Structure 4*, 1441−1452.
35. Burmeister, W. (2000) *Acta Crystallogr. D56*, 328−341.
36. Fujimoto, Z., Takase, K., Doui, N., Momma, M., Matsumoto, T., and Mizuno, H. (1998) *J. Mol. Biol. 277*, 393−407.
37. Dowd, M. K., French, A. D., and Reilly, P. J. (1994) *Carbohydr. Res. 264*, 1−19.
38. Feller, G., Payan, F., Theys, F., Qian, M., Haser, R., and Gerday, C. (1994) *Eur. J. Biochem. 222*, 441−447.
39. McIntosh, L. P., Hand, G., Johnson, P. E., Joshi, M. D., Körner, M., Plesniak, L. A., Ziser, L., Wakarchuk, W. W., and Withers, S. G. (1996) *Biochemistry 35*, 9958−9966.
40. Kraulis, P. J. (1991) *J. Appl. Crystallogr. 24*, 946−950.
41. Roussel, A., and Cambillau, C. (1989) in *Silicon Graphics geometry partner directory (Fall 1989)* (Silicon Graphics, Ed.) pp 77−78, Silicon Graphics, Mountain View, CA.

BI0102050